

Dual-Frequency Smoothing for CAT III LAAS: Performance Assessment Considering Ionosphere Anomalies

Hiroyuki Konno, *Stanford University*

BIOGRAPHY

Hiroyuki Konno is a Ph.D. candidate in Aeronautics and Astronautics working with the GPS Laboratory at Stanford University. His current research interest is in Local Area Augmentation System (LAAS) using dual-frequency GPS techniques. He received his B.S. in Mechanical Engineering in 1994 from Osaka University, Japan; his M.S. in Computer Science in 1996 from Nara Institute of Science and Technology, Japan; and his M.S. in Aeronautics and Astronautics from Stanford University in 2003.

ABSTRACT

Strong ionosphere storms are the most-threatening potential fault mode for the Local Area Augmentation System (LAAS). Multi-frequency GPS techniques are known to be an effective means of reducing or removing ionosphere-induced problems. Among those techniques, of great interest are Divergence-Free smoothing (denoted here as DFree) and Ionosphere-Free smoothing (denoted here as IFree). This paper discusses the practical benefit of these methods in the context of Category III LAAS.

First, this paper discusses a dual-frequency LAAS that implements DFree. Although DFree significantly mitigates the threat of ionosphere anomalies as compared to single-frequency carrier smoothing that is employed in conventional LAAS, the remaining threat must be addressed to meet the stringent integrity requirement of CAT III landing. This paper uses an ionosphere monitoring method to detect conditions in which the residual risk is unacceptable and evaluates the long-term system availability of the resulting DFree-plus-monitoring method. Simulations show that this approach achieves more than 99.9% availability at more than 50% of the Conterminous United States (CONUS).

Next, this paper discusses a dual-frequency LAAS that implements both DFree and IFree. By definition, IFree is completely immune to all ionosphere-related problems; however, it cannot be nominally used in LAAS because of the large error size of the smoothed signals. This paper

discusses the use of IFree as a backup in case of ionosphere anomaly under which DFree LAAS would otherwise be unavailable. In particular, the trigger conditions at which the system should switch from DFree to IFree are studied from the view point of maximizing system availability.

1. INTRODUCTION

The Local Area Augmentation System (LAAS) assumes near-perfect correlation of the ionosphere delays between a LAAS Ground Facility (LGF) and its users, so that these users can cancel out the ionosphere delays from their measurements by using differential corrections broadcasted by the LGF. However, extreme ionosphere storms which created large ionosphere differences over short baselines have been discovered over the Conterminous United States (CONUS) [1,2,3,4]. Studies of these events have shown that, if such a storm hits an LGF, differential ranging errors due to ionosphere delay differences between the LGF and users could exceed 3 – 5 meters [2,3]. Hence, severe ionosphere anomalies are now regarded as the most threatening fault mode to LAAS.

For LAAS for Category I (CAT I) precision landing, Lee *et al* proposed the “position-domain geometry screening” method and confirmed that this method achieved 99.9% long-term availability at several airports [5]. To obtain this level of availability, they used a variation of the Vertical Alert Limit (VAL) called $VAL_{H2,I}$ whose value was 24 m at 5 km from LGF. Although they claimed that this level of VAL could be safe enough for CAT I landing, it will not be so for CAT III landing. Therefore, developing a method that achieves reasonable availability with a much smaller VAL, for example 10 meters, is a critical challenge for CAT III LAAS.

To confront this technical challenge, this paper examines multi-frequency GPS techniques that are known to be an effective means to reduce or remove ionosphere-induced errors [6,7]. Among those techniques, of great interest to LAAS are Divergence-Free smoothing (DFree) and Ionosphere-Free smoothing (IFree) introduced by Hwang, McGraw, and Bader [8]. These methods are based on the

same concept as single-frequency carrier smoothing employed in conventional LAAS, which is a well-known technique that uses precise but biased carrier-phase measurements to smooth noisy but absolute code measurements. The use of dual-frequency measurements in DFree and IFree significantly reduces the effect of ionosphere errors from which single-frequency carrier smoothing suffers.

The main difference between DFree and IFree is the degree to which ionosphere effects are removed from the smoothed signals. DFree eliminates the effect of ionosphere divergence in the smoothing process while keeping the noise level the same as that of single-frequency carrier smoothing. Instantaneous ionosphere delays, however, remain in the smoothed signals. IFree, on the other hand, removes all ionosphere delays from the smoothed signals; hence, it is completely immune to ionosphere-related problems. However, as a side-effect of complete removal of ionosphere delay, the noise level of the smoothed signals is significantly larger than that of DFree [8].

This paper first examines the LAAS employing DFree and evaluates its long-term availability. Previous studies have conducted similar availability evaluations in the context of DGPS using DFree [9,10]. However, they did not take potential ionosphere anomalies into account. As described above, DFree has instantaneous ionosphere delays in its output; hence, extremely large ionosphere gradients such as those mentioned above and in [1,2,3,4] are still a potential threat. An integrity monitoring strategy for this threat is thus required to meet the stringent integrity requirement for CAT III LAAS [11]. Previous work by this author in [12] introduced an ionosphere monitoring method to be used with DFree and derived a Vertical Protection Level (VPL) which is a conservative navigation error bound that accounts for the performance of this method. This VPL allows the evaluation of availability of DFree LAAS that provides a sufficient integrity guarantee against ionosphere anomalies. The work in [12] evaluated the long-term availabilities at three airports (Memphis, LA, and NY) using this VPL. This paper expands the area of the availability evaluation to all over CONUS and shows that the DFree-plus-monitoring method achieves more than 99.9% availability at more than 50% of CONUS with 10-meter VAL.

Next, the paper discusses the use of IFree. Previous work by this author in [13] showed that a system which nominally used IFree could not achieve acceptable availability due to its large nominal-error level. However, IFree, with its immunity against ionosphere errors, might enable the system to provide service during ionosphere storms that prevent the system using DFree from providing safe service. Studies such as [13,14] have introduced the idea of implementing both DFree and IFree in LAAS and switching between them based on the best estimate of the

current ionosphere condition. In particular, McGraw proposed a sophisticated DGPS architecture which can switch between DFree and IFree in real time [14]. These studies, however, did not address at what condition the system should switch from DFree to IFree. This paper discusses the proper switching point from the view point of maximizing system availability under conservative assumptions regarding the ionosphere anomaly threat to CAT III user integrity.

Note that, given the choice of three possible dual-frequency combinations (L1/L2, L2/L5, and L1/L5), this paper focuses on the L1/L5 combination. This is because, unlike the L2 signal, the L1 and L5 signals are protected for aviation use, as they reside in Aeronautical Radio Navigation Service (ARNS) bands. However, all methods described in this paper are applicable for all three dual-frequency combinations.

2. LANDING OPERATION AND IONOSPHERE THREAT

Before discussing the details of the proposed dual-frequency LAAS algorithms, it is important to clarify the landing operation assumed in this paper. LAAS provides guidance on landing for its users up to a “decision point” beyond which the pilot and other sensors provide guidance to touchdown. In this paper, the decision point is set to 5 km from the LGF, and the user passes the point with a velocity of 0.07 km/sec. This landing operation is illustrated in Figure 1.

This paper also assumes that the anomalous ionosphere that affects landing is described by an ionosphere threat space model having three parameters: spatial gradient, velocity with respect to the ground, and width. This model is

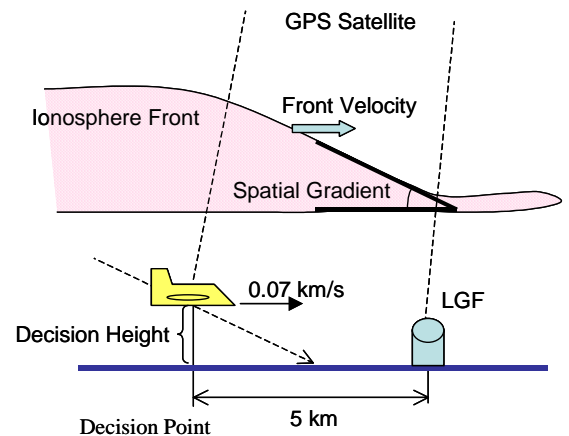


Figure 1: Illustration of landing operation with ionosphere front

essentially the same as the “ionosphere anomaly threat model” for CAT I LAAS [4,5]. Considering the more stringent integrity requirements for CAT III LAAS [11], this paper allows for extra margin in the gradient as compared to the CAT I model and sets the maximum gradient to 400 mm/km for all elevation angles. The parameter ranges for the model are shown in Table 1.

Table 1: Parameter ranges in ionosphere threat model

| Parameter | Range | Note |
|-----------|------------------|--------------------|
| Gradient | 35 ~ 400 (mm/km) | for all elevations |
| Velocity | 0 ~ 0.75 (km/s) | -- |
| Width | 25 ~ 100 (km) | -- |

3. OUTLINE OF LAAS WITH DIVERGENCE-FREE SMOOTHING

This section describes the outline of Divergence-Free (DFree) LAAS as proposed in [12]. First, the theory of DFree is briefly reviewed (detailed explanations can be found in [8,12,13]). In the review, DFree and single-frequency carrier smoothing are compared to make the advantages of DFree clear. Next, this section describes an ionosphere monitoring method that is very sensitive to anomalous ionosphere but suffers from a particular undetectable condition, which is described in detail. Finally, a Vertical Protection Level (VPL) considering the characteristics of DFree and the ionosphere monitor is derived.

3.1 Divergence-Free Smoothing (DFree)

DFree and single-frequency carrier smoothing have the same filter structure shown in Figure 2. Here, Ψ represents the input signal containing code measurements, Φ represents the input signal containing carrier-phase measurements, and τ (in the transfer function of the low-pass filter) is the smoothing time constant, which is normally set to 100 seconds in single-frequency LAAS [11,15].

Single-frequency carrier smoothing uses the L1 code measurement, ρ_1 , for Ψ and the L1 carrier-phase measurement, ϕ_1 , for Φ . They are modeled as follows.

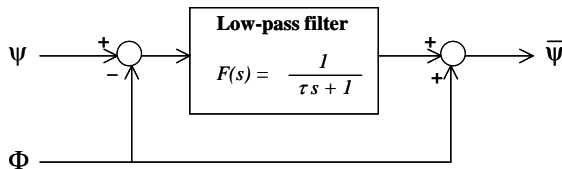


Figure 2: Block diagram of smoothing filter

$$\begin{aligned}\Psi &= \rho_1 = r + I_1 + \eta_1 \\ \Phi &= \phi_1 = r - I_1 + N_1\end{aligned}\quad (1)$$

Here, r includes all terms common to both code and carrier measurements, such as actual range to the satellite, clock offsets, and troposphere delay. I_1 represents the ionosphere delay, η_1 is the random noise on code measurements (e.g., thermal noise and multipath), and N_1 is the integer ambiguity of the carrier measurements. Random noise on carrier measurements is ignored, since it is much smaller than noise on code measurements. The subscript “1” indicates that the measurements are on the L1 frequency.

The DFree method feeds L1 code and L1/L5 carrier measurements into the smoothing filter. These inputs are expressed as follows.

$$\begin{aligned}\Psi &= \rho_1 = r + I_1 + \eta_1 \\ \Phi &= \phi_1 - \frac{2}{\alpha}(\phi_1 - \phi_5) \\ &= r + I_1 + N_1 - \frac{2}{\alpha}(N_1 - N_5) + \frac{2}{\alpha}(IFB + \tau_{gd}),\end{aligned}\quad (2)$$

where $\alpha = 1 - f_{L1}^2 / f_{L5}^2$.

Here, IFB is the interfrequency bias of the receiver which is typically caused by hardware differences between L1 and L5 signal paths, τ_{gd} is the interfrequency bias of the satellite transmitter which is also caused by the L1/L5 hardware differences [16,17], and f_{L1} and f_{L5} are the L1 and L5 frequencies (1575.42 and 1176.45 MHz, respectively).

Expressed in terms of Laplace transforms, the output of single-frequency carrier smoothing is given as

$$\bar{\Psi}_{sfc} = r + (2F - 1)I_1 + F\eta_1, \quad (3)$$

and the output of DFree is given as

$$\bar{\Psi}_{DF} = r + I_1 + F\eta_1. \quad (4)$$

Here, F represents the transfer function of the low-pass filter. The second term on the right-hand side of these equations describes the ionosphere error on the output signal, and the third term represents the random noise on the output.

Comparing (3) and (4), two things are notable: first, the ionosphere errors of these outputs are different; and second, the noise levels of these outputs are identical. As equation (4) indicates, the ionosphere term of DFree is identical to the instantaneous ionosphere delays on raw-code measurements. In contrast, the ionosphere term of single-frequency carrier smoothing has a filtering influence

expressed as $(2F - 1)$. For example, suppose the ionosphere delay on raw-code measurements, $I(t)$, has a constant rate of change in time, I_d .

$$I(t) = I_d t + I_0 \quad (5)$$

Ionosphere errors on the DFree output, $I_{DF}(t)$, are identical with those on raw-code measurements,

$$I_{DF}(t) = I(t); \quad (6)$$

whereas those on single-frequency carrier smoothing, $I_{sfc}(t)$, become the following.

$$I_{sfc}(t) = I(t) - 2\tau I_d. \quad (7)$$

The second term, $-2\tau I_d$, is a delay effect that occurs when a time-varying ionosphere delay passes through the low-pass filter [8].

By getting rid of the time-varying delay effect while keeping the noise level the same, DFree significantly improves the robustness of LAAS against ionosphere anomalies in comparison to single-frequency carrier smoothing. However, because the instantaneous raw-code ionosphere delay remains in the output, ionosphere fronts that create large absolute differences in ionosphere delays between the LGF and the user are still a potential threat to DFree-based LAAS. The next section describes an ionosphere monitoring method that helps to mitigate this threat.

3.2 Ionosphere Monitoring Method

Previous work [12] introduced an ionosphere monitoring method in which ground and airborne monitors independently estimate instantaneous rates of change of ionosphere delay to detect satellites whose signals are most probably affected by anomalous ionosphere. The LGF broadcasts the results of its screening process to the user, and the user estimates its position excluding the faulted satellites identified by the combined results of ground and airborne monitoring.

This method first estimates the ionosphere delays using L1 and L5 carrier-phase measurements as follows.

$$\begin{aligned} \tilde{I}[k] &= \frac{1}{\alpha} (\phi_5[k] - \phi_1[k]) \\ &= I[k] + \frac{1}{\alpha} (N_{15}[k] + IFB + \tau_{gd}) + \frac{1}{\alpha} \varepsilon_{15}[k] \quad (8) \\ (N_{15} &= N_5 - N_1, \varepsilon_{15} = \varepsilon_5 - \varepsilon_1) \end{aligned}$$

Here, ε is the noise on the carrier-phase measurements. Assuming no cycle slips are detected, instantaneous rates of

change of these delays are computed as follows.

$$\tilde{I}_{raw}[k] = \frac{1}{qT_{id}} (\tilde{I}[k] - \tilde{I}[k - q]) = \dot{I}[k] + \dot{\varepsilon}_{15}[k] \quad (9)$$

Here, T_{id} is the sampling period of the carrier-phase measurements, which is set to 0.5 seconds; q is an arbitrary integer that is set to 2 (setting it to 2 looks 2 epochs or 1 second backward in time). The raw rates from (9) are then fed into a low-pass filter to reduce the noise.

$$\hat{I}[k] = \frac{\tau_{id} - 1}{\tau_{id}} \hat{I}[k - 1] + \frac{1}{\tau_{id}} \tilde{I}_{raw}[k] \quad (10)$$

Here, τ_{id} is the time constant for the low-pass filter, which is set to 20 seconds.

The smoothed ionosphere rate, $\hat{I}[k]$, is the test statistic of this method, and satellites whose test statistic exceeds a threshold are detected as “faulted” (more precisely, impacted by anomalous ionosphere) satellites. Figure 3 shows the threshold specified by analyzing empirical data collected by a L1/L2 dual-frequency receiver at Stanford University. This threshold is given such that the theoretical probability of a fault-free alarm becomes less than 1.98×10^{-9} , which is considered sufficient for the continuity requirement for CAT III LAAS [11]. Details of the process to develop this threshold are found in [12].

Note that the threshold depicted in Figure 3 is determined based on the analysis of L1/L2 data sets. It makes sense to repeat this data analysis using L1/L5 data when implementing the above method with L1/L5 measurements. However, the only difference that will appear between the L1/L2 and L1/L5 data analyses is the effect of carrier noise (ε_{12} and ε_{15}), and this difference should be very small. Therefore, the threshold based on L1/L5 data should be very similar to that shown in Figure 3.

Because carrier-phase noise is very small to begin with, the test statistic is precise enough to have a very tight threshold

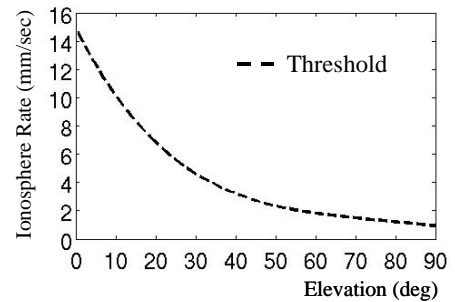


Figure 3: Threshold of ionosphere monitor

and, as a consequence, this monitor is very sensitive in detecting most ionosphere anomalies. However, there exists a particular condition to which the monitor is theoretically insensitive. The next subsection describes this undetectable condition.

3.3 Undetectable Ionosphere Fronts and the Worst-Case Scenario for the Monitoring Method

A fundamental problem of the ionosphere monitoring method is that it observes temporal gradients rather than spatial gradients or (better yet) absolute differences of ionosphere delays between the LGF and the user. If an ionosphere front that induces a large differential range error looks stationary from the point of view of the monitor, it is very difficult to detect.

Suppose an ionosphere front with a spatial gradient of α (mm/km) is affecting signals from a satellite observed by the monitor. Denoting the relative velocity between the front and the ionosphere-pierce-point (IPP) as $dV_{front/IPP}$ (km/sec), the relationship between the ionosphere rate observed by the monitor and the ionosphere spatial gradient is given as follows.

$$\frac{dI}{dt} = \alpha \cdot dV_{front/IPP} \quad (11)$$

This linear model transforms the detection threshold on ionosphere rates shown in Figure 3 into a threshold in the domain of spatial gradients. Figure 4 shows this spatial-gradient threshold as a function of $dV_{front/IPP}$ given an elevation angle. As shown in the figure, all ionosphere fronts with $dV_{front/IPP}$ of zero—fronts synchronized with the IPP—exist below the detection threshold regardless of the gradient and the elevation angle. Because fronts below the threshold are unlikely to be detected, fronts synchronized with the IPP are very difficult for the monitor to detect.

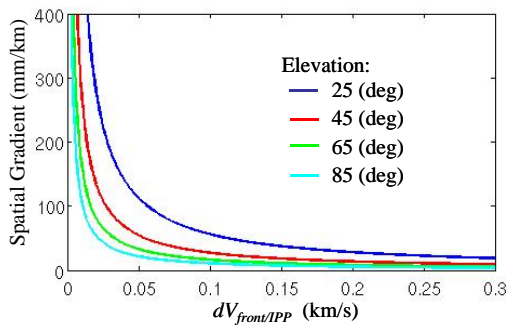


Figure 4: Threshold of spatial gradients as a function of $dV_{front/IPP}$

Implementing the monitor in both of the user and the LGF partially compensates for this weakness against the synchronized movement of fronts and IPPs. Because the user is an aircraft that is approaching the stationary LGF at a velocity of about 0.07 km/sec at the decision point, user's IPP has a different velocity from the associated IPP as seen by the LGF. Hence, if a front is synchronized with the IPP of the user, the front must have a relative velocity of about 0.07 km/sec with respect to the IPP for the LGF, and vice versa. As shown in Figure 4, $dV_{front/IPP}$ of 0.07 km/sec is high enough for the monitor to detect most threatening fronts. Therefore, anomalous fronts that cover both IPPs for the user and the LGF will be detected by either of the airborne or the ground monitor, if not both monitors.

Despite this constraint, a small set of undetectable fronts for this method remains: they are fronts that move with the IPP of the user (or the LGF) and hit the IPP of the LGF (or the user) just as the user passes over the decision point. As shown in Figure 5, if a front satisfies this condition, the airborne monitor cannot detect the front due to the synchronization, and the ground monitor cannot detect the front because its IPP does not “catch up to” the front before the user passes the decision point.

This undetectable condition can also be applied to the case where a front affects more than one satellite. Figure 6 (A) illustrates a geometry in which a front affects two satellites and satisfies the undetectable condition. The airborne monitor cannot detect the front because both IPPs affected by the front (blue circles) move with the front. In addition, because the edge of the front is less than 5 km from the user's IPPs, the IPPs for the LGF (red circles) do not catch up to the front before the user passes over the decision point; thus, the ground monitor cannot detect the front. Similarly, Figure 6 (B) shows the undetectable condition for the front affecting three satellites. Under this condition,

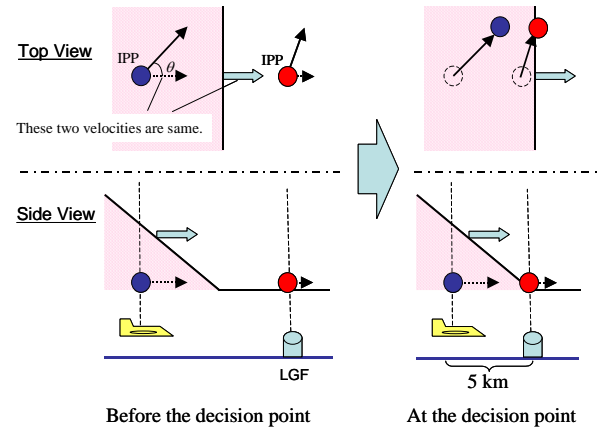


Figure 5: Illustration of undetectable condition for ionosphere monitoring method

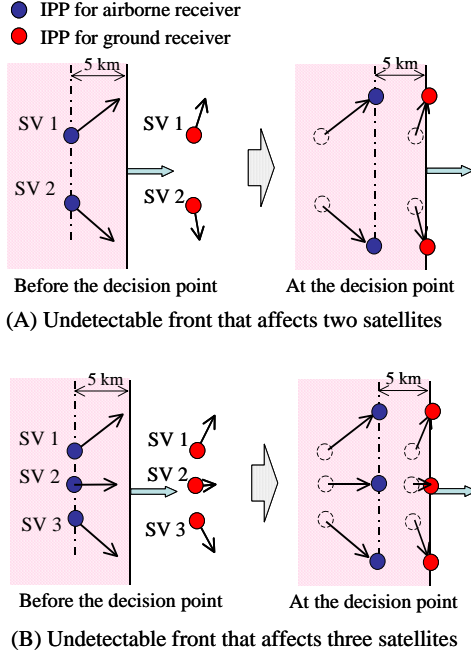


Figure 6: Undetectable front that affects more than one satellite

the monitoring method will miss detecting the front for the same reason as the two-satellite case.

As shown above, it is easy to construct theoretical conditions for undetectable fronts that affect multiple satellites. However, being able to construct theoretical conditions does not mean that such situations can actually occur. Figure 6 implies that the geometry of IPPs that could suffer from undetectable fronts is very improbable. Previous work [18] investigated actual satellite geometries for three airports (Memphis, LA, and NY) to confirm if such special conditions would happen in practice. In this investigation, several IPP pairs that had the potential to suffer from an undetectable-front condition were found. On the other hand, no IPP triplet whose geometry could satisfy the undetectable condition was found. Based on this result, it was concluded that missed-detection of ionosphere fronts affecting two satellites could occur; however, missed-detection of fronts affecting more than two satellites is extremely improbable. The worst-case scenario for the monitor is, therefore, defined as follows.

Worst-case scenario: A situation where an ionosphere front with the maximum gradient affects two satellites without being detected by the ionosphere monitor.

The next subsection derives a theoretical VPL_{iono} that models this condition.

3.4 Derivation of VPL_{iono}

VPL_{iono} represents a conservative bound on the theoretical vertical navigation error, E_{iono} , induced by the undetected ionosphere anomaly wave front. The navigation error, E_{iono} , is the sum of the random error associated with nominal ranging measurements and the bias error caused by the undetected front. The probability distribution of this error is given as follows.

$$p(E_{iono}) \sim \mathcal{N}(Bias, \sigma_v^2) \quad (12)$$

Here, $Bias$ represents the bias error due to the undetected front, and σ_v is the standard deviation of the random navigation errors, which is modeled as

$$\sigma_v = \sqrt{\sum_{k=1}^N S_{v,k}^2 (\sigma_{DF_gnd,k}^2 + \sigma_{DF_air,k}^2 + \sigma_{iono,k}^2)} \quad (13)$$

Here, σ_{DF_gnd} and σ_{DF_air} are the standard deviations of errors associated with the ground and the airborne receivers that execute DFree smoothing, and σ_{iono} is the error caused by the nominal ionosphere gradient. The index k represents satellite k ($k = 1, 2, \dots, N$ satellites in view). In this paper, errors due to troposphere decorrelation are ignored because they are very small by comparison [15]. The terms $S_{v,k}$ are the relevant coefficients from the weighted pseudoinverse range-to-position transformation matrix S [11].

VPL_{iono} is determined such that the probability of loss of integrity due to the ionosphere fault does not exceed the allowable integrity risk for the fault. Loss of integrity involves three events: first, an ionosphere anomaly occurs; second, the ionosphere monitor fails to detect the anomaly; and finally, VPL_{iono} fails to bound the fault-induced error. Each of these events has a probability: P_{iono} , the prior probability of ionosphere anomalies; P_{md} , the conditional probability of missed detection by the ionosphere monitor given the existence of the anomaly; and P_{pl} , the conditional probability that the error exceeds the protection level given that an anomaly exists and that missed-detection occurs. To meet integrity, the product of these probabilities must not exceed the allowable integrity risk for the ionosphere fault, P_a .

$$P_a \geq P_{pl} P_{md} P_{iono} \quad (14)$$

From this constraint, the maximum allowable risk that the error exceeds the protection level given that the monitor has failed to detect the anomaly is expressed as

$$P_{pl}^* = \frac{P_a}{P_{md} P_{iono}} \quad (15)$$

VPL_{iono} is determined such that the risk of a vertical positioning error exceeding it does not surpass the maximum allowable risk given by (15) while the ionosphere behavior is monitored. Hence, given the distribution of the vertical positioning error from equation (12), the value of VPL_{iono} can be determined by integrating this probability density up to the point that the probability of error exceeding VPL_{iono} becomes the allowable risk P_{pl}^* .

$$VPL_{iono} = -Q^{-1}\left(\frac{P_a}{P_{md}P_{iono}}\right)\sigma_v + Bias \quad (16)$$

Figure 7 schematically expresses the relationship between VPL_{iono} and the distribution of the positioning error. The bell-shape curve shows the error distribution given an ionosphere front which the monitor has failed to detect (equation (12)). The Q-function in equation (16) represents the cumulative probability in the tail of the Gaussian error distribution outside the VPL_{iono} . Strictly, tails on both sides of the distribution should be taken account. However, the total probability in one of these tails is negligible as compared with the probability in the other. Hence, in equation (16), only one tail is considered, and the allowable risk, P_{pl}^* , is assigned to this tail. Note that equation (16) represents the general form of VPL_{iono} . The remainder of this section specifies $Bias$ and the three probabilities (P_a , P_{md} , and P_{iono}), considering the worst-case scenario described in Section 3.3.

Recall that the worst-case scenario for the DFree system with the proposed monitor is that an ionosphere front with the maximum gradient simultaneously affects two satellites without being detected by the monitor. The bias corresponding to this condition is given as follows.

$$Bias_{max} = \max\left(\max_i(|S_{v,i}|\Delta I_{max}), \max_{i,j}(|S_{v,i} + S_{v,j}|\Delta I_{max})\right) \quad (17)$$

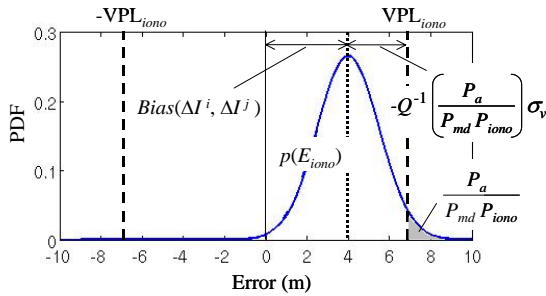


Figure 7: Distribution of positioning error and VPL_{iono}

Here ΔI_{max} is the maximum differential range error induced by the front, which in this paper is set to 2 m (the maximum spatial gradient of 400 mm/km times the user-to-LGF separation of 5 km at the decision point). In most cases, the maximum error of the two-satellite-affected situation—the second argument of the outer $\max(\bullet)$ in equation (17)—is larger than that of one-satellite-affected situation, which is given by the first argument of the outer $\max(\bullet)$ in (17). Taking the maximum between them takes account of geometries like the one whose S_v is, for example, given as $S_v = [-2.12, 0.67, 0.54, 0.03, 0.88]$. In this example, the maximum bias for the two-satellite-affected situation is 4.18 m, while that for the one-satellite-affected situation is 4.24 m.

The integrity risk allocated to ionosphere faults, P_a , is a sub-allocation from the overall system integrity requirement. Because this value would normally be chosen by the LGF system designer, a P_a value of 10^{-10} , or 10% of the total CAT III integrity requirement of 10^{-9} per approach [11], is used in this paper.

Under the worst-case condition, the probability of missed-detection, P_{md} , is the probability that the monitoring method misses detecting an ionosphere front affecting two satellites. As discussed in the previous section, front detectability depends on the relative velocity between the front and the IPP ($dV_{front/IPP}$), which is a quantity that the monitor cannot observe. Hence, P_{md} cannot be explicitly determined. In other words, it is impossible to estimate how often an ionosphere front is synchronized with an IPP. Although P_{md} might be very small because synchronization is extremely rare, this paper conservatively sets it to 1 considering the stringent integrity requirement for CAT III LAAS. By setting the probability of missed-detection to 1, it may appear that the monitor does not contribute to mitigation of ionosphere risk. In fact, the method has already contributed by reducing the set of ionosphere threats to cases in which no more than two satellites are simultaneously affected by an ionosphere front.

The prior probability of an ionosphere anomaly, P_{iono} , is a controversial parameter in the LAAS community [19]. Previous work [12] employed P_{iono} of 1 for conservatism, which seems extremely conservative given the known rarity of significantly anomalous ionosphere conditions. This paper uses a more reasonable value derived from [20]. In [20], Pullen *et al* investigated databases of ionosphere events and derived prior probability estimates based on the fraction of days in which gradients large enough to threaten LAAS might occur. Applying some mitigating conditions to this baseline probability, it estimated P_{iono} of 10^{-6} as a sufficiently conservative value. This paper adds extra conservatism and sets P_{iono} to 10^{-5} .

Substituting $Bias_{max}$ and these three probabilities into equation (16), VPL_{iono} is finally given as follows.

$$\begin{aligned} \text{VPL}_{iono} &= -Q^{-1}\left(\frac{10^{-10}}{10^{-5}}\right)\sigma_v + \text{Bias}_{\max} \\ &= 4.265\sigma_v + \text{Bias}_{\max} \end{aligned} \quad (18)$$

The proposed ionosphere monitor and VPL_{iono} can be easily implemented into the LAAS architecture. In conventional LAAS, the LGF broadcasts the error bound for each satellite, $\sigma_{gnd,k}$, to approaching users which compute their own VPL to decide whether or not to complete their individual landing operations. To obtain this VPL, the airborne users evaluates several VPLs based on different state hypotheses (such as H_0 , the fault-free hypothesis) and selects the largest VPL among these hypotheses as the VPS to be used for the current operation [11]. VPL_{iono} is newly included and is simply added to this computation as a VPL equation corresponding to the ionosphere-fault hypothesis.

4. AVAILABILITY SIMULATION FOR DFREE LAAS

This section introduces the results of the availability simulations conducted to evaluate the practical benefit of DFree LAAS described in the previous section. First, the way to compute long-term system availability is explained; then, the simulation results are discussed.

4.1 Availability Computation

“Long-term” system availability is defined as the average of “instantaneous” availability for one 24-hour day of repeatable GPS geometries and is computed as follows.

$$P_{avail} = \sum_{l=1}^L \frac{1}{L} \left[\sum_{U=0}^4 \sum_{m=1}^{M(U)} \frac{P_{SVout}(U)}{M(U)} P_{avail-idx}(\lambda_m(t_l, U)) \right] \quad (19)$$

Here, $P_{avail-idx}(\lambda_m(t_l, U))$ is an availability indicator valuable for a satellite geometry denoted by $\lambda_m(t_l, U)$, where t_l ($l = 1, \dots, L$) represents one epoch of time, and U corresponds to the number of unavailable satellites at t_l . The availability indicator takes a value of 1 if the system is available for the geometry in question; otherwise, it takes a value of 0. The way to decide the value of the indicator will be described later.

The term inside the brackets in equation (19) represents instantaneous availability at a particular epoch. Instantaneous availability is a weighted-average of the availability indicators for all possible satellite geometries during the chosen epoch. Here, “all possible” means considering not only the geometry where all satellites are working but also geometries in which one or more satellites are under scheduled or unscheduled downtime. $M(U)$ is the number of satellite combinations that occur for the U -satellite-out condition (i.e., $M(U)$ is “ N choose U ” for a constellation of N satellites). For each of these $M(U)$

combinations, a geometry of usable satellites, $\lambda_m(t_l, U)$, is defined; then, the availability indicator for the geometry, $P_{avail-idx}(\lambda_m(t_l, U))$, is determined. The instantaneous availability is computed by averaging these availability indicators with the weighting factor $P_{SVout}(U)/M(U)$. Here, $P_{SVout}(U)$ is the probability that U satellites are experiencing scheduled or unscheduled downtime. Finally, the instantaneous availabilities are uniformly averaged for all epochs (t_l : $l = 1, \dots, L$). In this paper, instantaneous availability is computed every 5 minutes through one 24-hour day; hence, there are 288 epochs (i.e., $L = 288$ in equation (19)).

For each satellite geometry, the availability indicator is determined as follows.

$$\begin{aligned} P_{avail-idx}(\lambda_m) &= \begin{cases} 1 & \text{if VAL} \geq \text{VPL}_{DF} \\ 0 & \text{otherwise} \end{cases} \\ \text{VPL}_{DF} &= \max(\text{VPL}_{H_0}, \text{VPL}_{iono}) \end{aligned} \quad (20)$$

Here, VAL is the Vertical Alert Limit, and VPL_{H_0} is the VPL for the fault-free hypothesis, which is given as follows [11].

$$\text{VPL}_{H_0} = K_{ffmd} \sigma_v \quad (21)$$

($K_{ffmd} = 6.673$ for CAT III LAAS using 4 ground receivers)

Currently, there is no universally agreed value for VAL for CAT III LAAS. Therefore VAL can be varied to observe the sensitivity of availability as a function of VAL. This paper, however, uses the VAL of 10 meters from [11] as a fixed value in all simulations.

4.2 Simulation Results and Discussions

In availability simulations, the measurements error bound is an important quantity that directly dictates the system availability. As equation (13) shows, this error bound depends on the ground and airborne receiver errors (σ_{DF_gnd} and σ_{DF_air}), and errors due to nominal ionosphere gradients (σ_{iono}). Because the receiver noise in DFree is as large as that of single-frequency carrier smoothing (see Section 3.1), the Airborne Accuracy Designator (AAD) and the Ground Accuracy Designator (GAD)—error models developed for LAAS single-frequency carrier smoothing [11,15]—are just as suitable as the error model for DFree receivers. This paper uses AAD-B and GAD-C4 as baseline models (“C4” indicates that a 4-reference-receiver ground subsystem is assumed).

User differential range error due to nominal ionosphere spatial gradients is conventionally computed as follows.

$$\sigma_{iono,k} = d_{gu} \sigma_{vig} Oq^k \quad (22)$$

Here, d_{gu} is the distance between the user and LGF at the decision point (5 km in this paper), σ_{vig} is the nominal ionosphere spatial gradient in the zenith domain and is set to 5 mm/km, and Oq^k is the zenith-to-slant obliquity factor corresponding to the elevation angle of satellite k .

The satellite constellation is another important factor upon which availability simulations depend. In this paper, the 24-satellite GPS constellation on July 1, 1993 specified in [21] is used. One benefit of using this constellation is that the prior probabilities of satellite outages— $P_{svout}(U)$ in equation (19)—are fairly well known. This paper assigns the probabilities based on historical observations of the number of healthy satellites given in [21]. Table 2 lists these probabilities.

Table 2: Historical probabilities of satellite outages

| Unavailable Satellites, U , in 24 Satellite Constellation | Probability $P_{svout}(U)$ |
|--|-------------------------------|
| 0 | 0.983 |
| 1 | 0.006 |
| 2 | 0.010 |
| 3 | 0.001 |
| 4+ | 0 |

Using the baseline receiver models and the 24-satellite constellation, the author estimated long-term system availabilities at a grid of locations in CONUS separated by 2 degrees of latitude and longitude. The results are shown in Figure 8. More than 99.9% availability is obtained in the western and the northeastern region of the United States. However there exists a broad region in the southeast where availability is less than 99%. This region appeared to be disadvantaged with respect to satellite geometry compared to other regions.

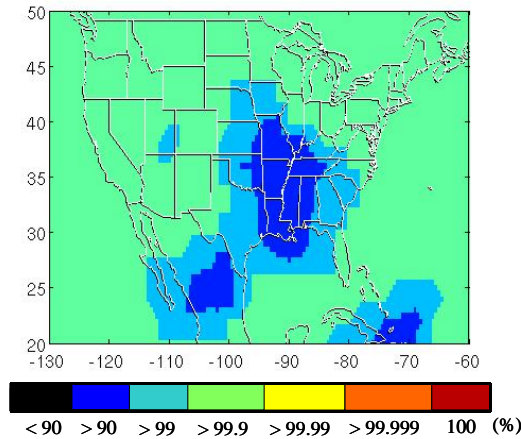


Figure 8: Availability of DFree LAAS

This paper has hitherto studied the DFree that uses L1 code measurement as the code input. It is of course possible to implement a variation of DFree that uses L5 code measurement as the code input, by replacing the L1 and L5 signals within the filter inputs (equation (2)). The output of this “L5-based” DFree is given as:

$$\overline{\Psi}_{L5DF} = r + I_5 + F\eta_5. \quad (23)$$

L5-based DFree smoothing has one key advantage and one key disadvantage. The advantage is that L5 code measurements will have a much smaller noise level compared with L1 code measurements due to higher signal power and a ten-times faster chipping rate [6], causing the output noise level of L5-based DFree, $F\eta_5$, to be much smaller than that of “L1-based” DFree, $F\eta_1$. The disadvantage is that, because the ionosphere error is in inverse proportion to the square of the signal frequency, the L5 ionosphere error, I_5 , is larger than the L1 ionosphere error, I_1 . The relationship between these two errors is:

$$I_5 = \frac{f_{L1}^2}{f_{L5}^2} I_1 \approx 1.8 I_1. \quad (24)$$

Because of this disadvantage, the “ $Bias_{max}$ ” term in the VPL_{iono} equation must be inflated. Specifically, in the $Bias_{max}$ equation (equation (17)), the maximum differential range error induced by the ionosphere front, ΔI_{max} , increases from 2 m to 3.6 m (i.e., by a factor of 1.8).

Considering this advantage and this disadvantage, system availability for the L5-based DFree method was estimated. To take the advantage into account, the simulation used receiver models of 0.5·AAD-B and 0.5·GAD-C4 based on the (optimistic) assumption that the standard deviation of L5 signal errors is half that of L1 errors. Figure 9 shows

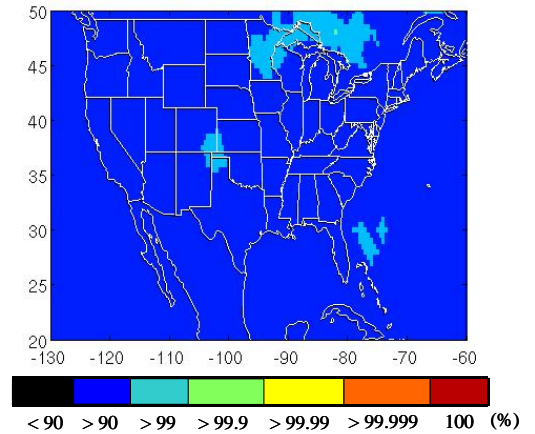


**Figure 9: Availability of L5-Based DFree LAAS
(based on assumption that $\sigma_{L5} = 0.5\sigma_{L1}$)**

the result, which clearly shows that the disadvantage of the large ionosphere errors on L5 measurements overwhelms the advantage in terms of receiver noise, resulting in unacceptably low availability even with optimistic receiver error models.

It is also important to understand that the simulations above estimate availability under nominal ionosphere conditions. If an ionosphere anomaly were to occur, the ionosphere monitor would exclude satellites affected by the anomaly. The resulting deterioration of usable satellite geometry inflates VPL and, at some point, makes the system unavailable. Consequently, under ionosphere anomalies, DFree LAAS cannot retain the high availability shown above. The next section discusses the use of IFree as a backup for DFree to maintain high availability during ionosphere anomalies.

5. USE OF IFREE AS A BACKUP METHOD

Recall from Section 1 that the IFree method completely removes ionosphere delay from the smoothed signals; thus, it is immune to ionosphere-related problems. Hence, it has potential as a backup to DFree under anomalous ionosphere conditions where DFree may not be available. This section discusses the concept of LAAS implementing both DFree and IFree and switching between them based on the ionosphere condition. First, the theory of IFree is briefly reviewed (a detailed explanation can be found in [8]); then, the system availability achieved by IFree under ionosphere anomalies is estimated. Finally, this section discusses what condition or threshold point should trigger the system to switch from DFree to IFree.

5.1 Ionosphere-Free Smoothing (IFree)

IFree has the same filter structure as DFree and single-frequency carrier smoothing (the structure shown in Figure 2) and feeds the following signals into the filter:

$$\begin{aligned}\Psi &= \rho_1 - \frac{1}{\alpha}(\rho_1 - \rho_5) \\ &= r + \eta_1 - \frac{1}{\alpha}(\eta_1 - \eta_5) + \frac{1}{\alpha}(IFB + \tau_{gd}) \\ \Phi &= \phi_1 - \frac{1}{\alpha}(\phi_1 - \phi_5) \\ &= r + N_1 - \frac{1}{\alpha}(N_1 - N_5) + \frac{1}{\alpha}(IFB + \tau_{gd})\end{aligned}\quad (25)$$

The smoothed signal is given as follows.

$$\bar{\Psi}_{IF} = r + F\left(\eta_1 - \frac{1}{\alpha}(\eta_1 - \eta_5)\right) + \frac{1}{\alpha}(IFB + \tau_{gd}) \quad (26)$$

Unlike DFree, the interfrequency terms (IFB and τ_{gd}) remain in the filter output. However, because the

interfrequency bias of the satellite, τ_{gd} , is cancelled through the DGPS process, and because the bias for the receiver, IFB , is included within the user receiver's clock offset during position estimation, these values have no effect on navigation.

The standard deviation of errors on IFree is expressed as follows, assuming that L1 and L5 errors are independent.

$$\sigma_{IF} = \sqrt{\left(1 - \frac{1}{\alpha}\right)^2 \sigma_{L1}^2 + \frac{1}{\alpha^2} \sigma_{L5}^2}. \quad (27)$$

Assume a hypothetical situation where the noise level of L5 code measurements is half that of L1 code ($\sigma_{L5} = 0.5\sigma_{L1}$), which is the same assumption as the one used for the L5-based DFree LAAS availability simulation in the previous section. Equation (27) becomes

$$\sigma_{IF} \approx 2.35\sigma_{L1}. \quad (28)$$

The ground and airborne receiver error models for IFree are given by substituting the existing Accuracy Designators (GAD and AAD) models into equation (28).

$$\begin{aligned}\sigma_{IF_gnd} &= 2.35 \cdot \text{GAD} - C4 \\ \sigma_{IF_air} &= 2.35 \cdot \text{AAD} - B\end{aligned}\quad (29)$$

Note that navigation errors for IFree LAAS do not depend on ionosphere decorrelation because the output of IFree includes no ionosphere-related quantities. Accordingly, the VPL of IFree LAAS, VPL_{IF} , can be constructed as follows (errors due to troposphere decorrelation are again ignored).

$$VPL_{IF} = K_{ffmd} \sqrt{\sum_{k=1}^N S_{v,k}^2 (\sigma_{IF_gnd,k}^2 + \sigma_{IF_air,k}^2)} \quad (30)$$

($K_{ffmd} = 6.673$ for CAT III LAAS using 4 ground receivers)

VPL_{IF} based on the assumption that $\sigma_{L5} = 0.5\sigma_{L1}$ is obtained by substituting the error models from (29) into (30).

5.2 IFree Availability under Ionosphere Anomalies

The availability of IFree LAAS can be estimated by using VPL_{IF} instead of VPL_{DF} in equation (20). Figure 10 shows the result of the resulting availability simulation. In the context of LAAS using IFree as a backup, this result can be interpreted as the anticipated availability which the system will achieve when affected by ionosphere anomalies. Overall, the availability, of course, decreases from that which DFree provides under nominal conditions (see Figure 8). However, considering the fact that DFree LAAS will most probably lose availability and stop providing service during anomalies, this level of availability

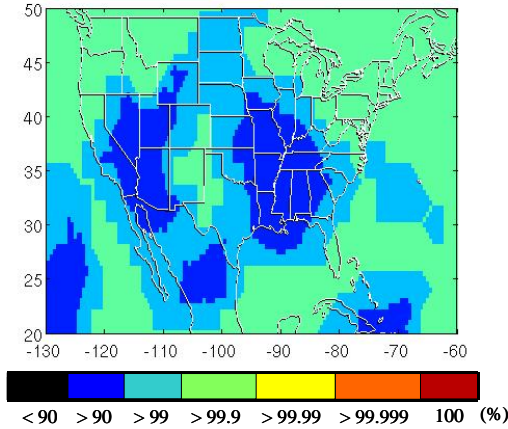


Figure 10: Availability of IFree LAAS
(based on assumption that $\sigma_{LS} = 0.5\sigma_{LI}$)

is attractive.

To fully obtain this advantage in practice, it is important to specify observable and viable conditions at which the system switches from DFree to IFree. The next subsection discusses this “switching point.”

5.3 Switching Point from DFree to IFree under Ionosphere Anomalies

The main objective of switching from DFree to IFree is to obtain the highest possible availability (consistent with integrity) during ionosphere anomalies. Hence, the optimal switching method is to evaluate VPL_{DF} and VPL_{IF} in parallel and select the method whose VPL is smaller, because VPL directly dictates the system availability. Under nominal conditions, VPL_{DF} is smaller than VPL_{IF} . However, once an ionosphere anomaly occurs and the ionosphere monitor excludes satellites affected by the anomaly, VPL_{DF} increases due to the deterioration of the usable satellite geometry. If the system switches to IFree, the excluded satellites can be reintroduced to the position estimation. Comparing VPL_{DF} after the exclusion and VPL_{IF} for the original geometry and then selecting the method having the smaller VPL, the system will be able to achieve maximum availability. The following example demonstrates this switching method.

Consider the satellite geometry illustrated in Figure 11, which is arbitrarily generated from the 24-satellite constellation from [21] used in the availability simulations. Azimuths and elevations of these satellites are listed in Table 3. If there is no faulted satellite excluded by the ionosphere monitor, namely under nominal ionosphere conditions, VPL_{DF} and VPL_{IF} are computed as 7.70 m and 8.71 m respectively. Now, suppose that an ionosphere front appears at the northeast corner of the sky and affects

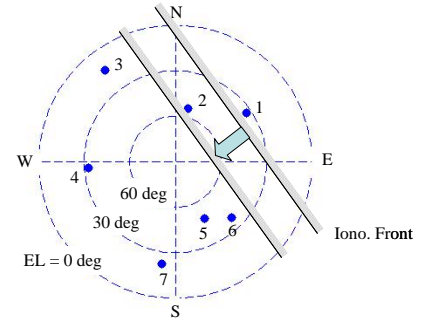


Figure 11: Sample 7-satellite geometry

Table 3: Locations of Each Satellite

| SV | Az (deg) | El (deg) | SV | Az (deg) | El (deg) |
|----|-------------|-------------|----|-------------|-------------|
| 1 | 55.60 | 33.48 | 5 | 152.80 | 48.16 |
| 2 | 13.52 | 54.14 | 6 | 134.76 | 37.58 |
| 3 | 322.51 | 14.14 | 7 | 187.62 | 22.31 |
| 4 | 266.15 | 32.52 | -- | -- | -- |

satellite 1 (see Figure 11), and that the ionosphere monitor excludes the satellite as a result. In this case, VPL_{DF} for the remaining satellites becomes 7.92 m, which is still smaller than the VPL_{IF} for the original geometry (8.71 m). Therefore, for this particular case, the system should keep using DFree to obtain the lowest possible VPL. Now suppose that, at a later time, the front has moved further to the southwest and has now affected satellites 1 and 2. VPL_{DF} for the remaining satellites at this later time becomes 10.75 m, which is now larger than VPL_{IF} (note that VPL_{IF} remains constant because it requires no satellite exclusions and is unaffected by ionosphere fronts). At this point, the system should switch to IFree.

A drawback of this method is that the system needs to evaluate both VPL_{DF} and VPL_{IF} at every epoch. An alternative method, which is much simpler, is to switch to IFree whenever a satellite is excluded by the ionosphere monitor without looking at VPL. Satellite exclusion by the ionosphere monitor signifies an ionosphere anomaly (or a monitor false-alarm); hence, it makes sense to switch to IFree for the remainder of the current operation regardless of VPL in order to avoid any problem due to the potential anomaly (recall that IFree is completely immune to ionosphere-related problems). The remainder of this section examines this switching method.

Because this simplified method does not consider VPL, in some cases, switching to IFree results in loss of availability compared to the optimal method. Specifically, if VPL_{DF} for the remaining satellites (after excluding one satellite) is less than VAL, and if VPL_{IF} for the original satellites exceeds VAL, then the system loses availability by

switching to IFree because it would have been available otherwise. If such losses occur frequently, this method is not worth the simplification gained. To analyze how much loss will be suffered by the simplified method, this paper defines the “advantaged sub-geometry” and the “disadvantaged sub-geometry.” Here, the phrase “sub-geometry” is used for the geometry comprised by the remaining satellites after the exclusion of one satellite. The “advantaged sub-geometry” is the sub-geometry that satisfies the following conditions.

- The sub-geometry is unavailable with DFree, namely $VPL_{DF} > VAL$.
- The system becomes available if it switches to IFree, namely $VPL_{IF} \leq VAL$ (here, VPL_{IF} is the one for the original geometry, with no satellite exclusions).

The “disadvantaged sub-geometry” is the opposite and is defined as follows.

- The sub-geometry is available with DFree, namely $VPL_{DF} \leq VAL$.
- The system becomes unavailable if it switches to IFree, namely $VPL_{IF} > VAL$.

For example, consider again the satellite geometry in Figure 11. There are 7 possible sub-geometries, whose VPL_{DF} values are listed in Table 4. The sub-geometry without satellite 2 and that without satellite 3 are advantaged sub-geometries because VPL_{DF} for them exceeds the VAL of 10 m while VPL_{IF} for the original geometry is less than VAL ($VPL_{IF} = 8.71$ m). The others are neither advantaged nor disadvantaged because the availability of the system is not changed by switching.

By counting the advantaged/disadvantaged sub-geometries for all original geometries over 24 hours, it can be determined how much gain or loss of availability will occur due to the simplified switching method. The author generated satellite geometries every 5 minutes assuming that all 24 satellites were healthy and counted these sub-geometries. Figures 12 and 13 show the counts of advantaged and disadvantaged sub-geometries, respectively, and Figure 14 shows their difference, namely, advantaged minus disadvantaged. Please note that the color assignments of these figures are different.

Table 4: VPL_{DF} for each sub-geometry

| | | | | |
|----------------|------|-------|-------|------|
| Excluded SV | 1 | 2 | 3 | 4 |
| VPL_{DF} (m) | 7.92 | 10.73 | 10.60 | 8.97 |
| Excluded SV | 5 | 6 | 7 | -- |
| VPL_{DF} (m) | 8.32 | 7.47 | 8.72 | -- |

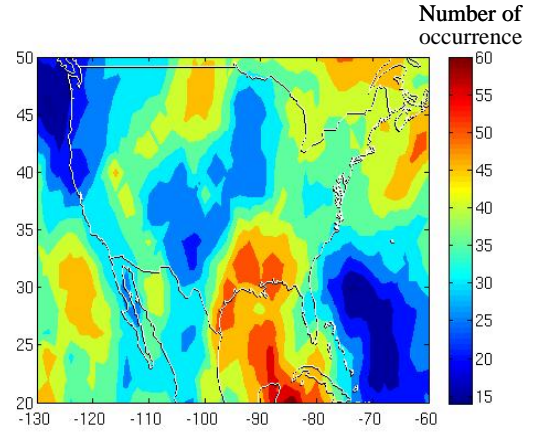


Figure 12: Count of advantaged sub-geometries

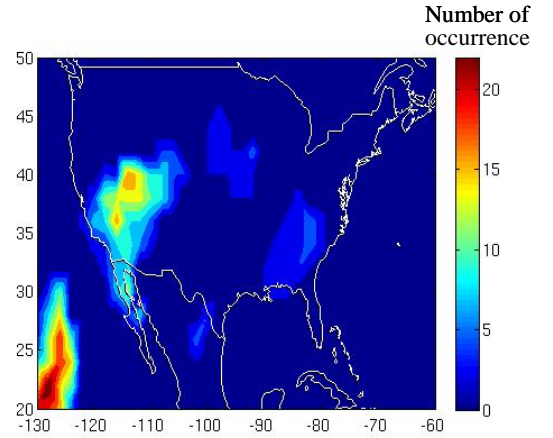


Figure 13: Count of disadvantaged sub-geometries

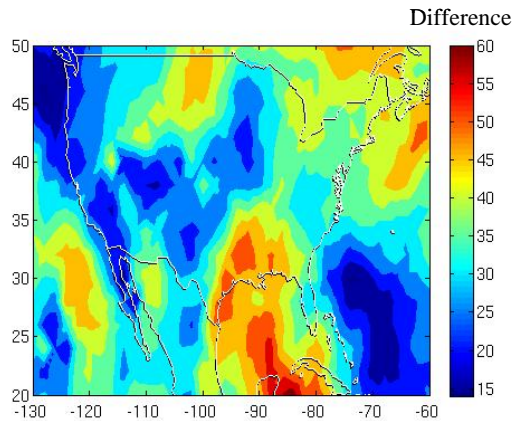


Figure 14: Difference of advantaged/disadvantaged sub-geometries

Figure 12 indicates that there are many advantaged sub-geometries. Recall that the definition of the advantaged sub-geometry has the condition that DFree is unavailable for that sub-geometry. Hence, this result implies that DFree LAAS will lose availability fairly often when a satellite is excluded due to anomalous ionosphere. In contrast, Figure 13 shows that few disadvantaged sub-geometries exist (and only in limited regions of CONUS). This means that switching to IFree based on the "one-satellite exclusion" rule will cause almost no loss of availability, compared to the optimal VPL-based method. Furthermore, Figure 14 shows that the number of advantaged cases surpasses that of disadvantaged all over CONUS. This shows that the simplified switching method is statistically beneficial.

6. CONCLUSIONS

This paper has assessed the performance of dual-frequency LAAS using divergence-free smoothing (DFree) that also performs monitoring for integrity against ionosphere anomalies. Simulations showed that, under nominal conditions, such a system would achieve more than 99.9% availability over a broad region in CONUS. Meanwhile, it also appeared that there existed a region in the southeast of CONUS where the availability would be less than 99%. This result suggests that this region has a disadvantage with respect to satellite geometry in compared to other regions. This paper also demonstrates the disadvantage of L5-based DFree, a variation of DFree that uses L5 code measurements for the code input as opposed to L1 code measurements. Because of the larger ionosphere error on L5 measurements, L5-based DFree cannot achieve acceptable availability with the integrity method described in this paper.

This paper has also discussed a variant of dual-frequency LAAS that implements both DFree and IFree and uses IFree as a backup during ionosphere anomalies. Availability simulations for this concept showed that, by using IFree, the system would achieve reasonably high availability even under ionosphere anomalies. One issue for this "hybrid" system is under what conditions the system should switch from DFree to IFree. This paper showed that a very simple method in which the system switches to IFree whenever the ionosphere monitor excludes a satellite would work effectively.

ACKNOWLEDGEMENTS

The constructive comments regarding this research provided by many people in the Stanford GPS laboratory are greatly appreciated. The author also acknowledges the Federal Aviation Administration LAAS Program Office for supporting this research. The opinions discussed here are those of the author and do not necessarily represent those of the FAA.

REFERENCES

- [1] S. Datta-Barua, T. Walter, *et al.*, "Using WAAS Ionospheric Data to Estimate LAAS Short Baseline Gradients," *Proceedings of ION National Technical Meeting*, Anaheim, CA., January 28-30, 2002.
- [2] M. Luo, S. Pullen, *et al.*, "Assessment of Ionospheric Impact on LAAS Using WAAS Supertruth Data," *Proceedings of The ION 58th Annual Meeting*, Albuquerque, NM., June 24-26, 2002.
- [3] M. Luo, S. Pullen, *et al.*, "LAAS Study of Slow-Moving Ionosphere Anomalies and Their Potential Impacts," *Proceedings of ION GNSS 2005*, Long Beach, CA., September 13-16, 2005.
- [4] A. Ene, Di Qiu, *et al.*, "A Comprehensive Ionosphere Storm Data Analysis Method to Support LAAS Threat Model Development," *Proceedings of ION National Technical Meeting*, San Diego, CA., January 15-20, 2005.
- [5] J. Lee, M. Luo, *et al.*, "Position-Domain Geometry Screening to Maximize LAAS Availability in the Presence of Ionosphere Anomalies," *Proceedings of ION GNSS 2006*, Fort Worth, TX., Sept. 26-29, 2006.
- [6] P. Enge, "GPS Modernization: Capabilities of the New Civil Signals," *Invited Paper for the Australian International Aerospace Congress*, Brisbane, July 29 – August 1, 2003.
- [7] S. Pullen, P. Enge, "A Civil User Perspective on Near-Term and Long-Term GPS Modernization," *Proceedings of Japan GPS/GNSS symposium 2004*, Tokyo Japan, November 17-19, 2004.
- [8] P. Hwang, G. McGraw, J. Bader, "Enhanced Differential GPS Carrier-Smoothed Code Processing Using Dual-Frequency Measurements," *Navigation*. Vol. 46, No. 2, Summer 1999, pp. 127-137.
- [9] C. Shively, T. Hsiao, "Availability Enhancements for CAT IIIB LAAS," *Navigation*. Vol. 51, No. 1, Spring 2004, pp. 45-57.
- [10] J. Stevens, C. Varner, *et al.*, "LDGPS Performance Assessment Using the JPALS Availability Model," *Proceedings of ION GNSS 2004*, Long Beach, CA., September 21-24, 2004.
- [11] *Minimum Aviation System Performance Standards for Local Area Augmentation System (LAAS)*. Washington, D.C., RTCA SC-159, WG-4A, DO-245A, Dec. 9, 2004.

[12] H. Konno, S. Pullen, *et al.*, "Ionosphere Monitoring Methodology for Hybrid Dual-Frequency LAAS," *Proceedings of ION GNSS 2006*, Fort Worth, TX., September 26-29, 2006.

[13] H. Konno, S. Pullen, *et al.*, "Evaluation of Two Types of Dual-Frequency Differential GPS Techniques under Anomalous Ionosphere Conditions," *Proceedings of ION National Technical Meeting*, Monterey, CA., January 18-20, 2006.

[14] G. McGraw, "Generalized Divergence-Free Carrier Smoothing with Applications to Dual Frequency Differential GPS," *Proceedings of ION National Technical Meeting*, Monterey, CA., January 18-20, 2006.

[15] G. McGraw, T. Murphy, *et al.*, "Development of the LAAS Accuracy Models," *Proceeding of ION GPS 2000*, Salt Lake City, UT., Sept. 19-22, 2000.

[16] H. Konno, S. Pullen, *et al.*, "Analysis of Ionosphere Gradient Using Japan GEONET Data," *Proceedings of ION National Technical Meeting*, San Diego, CA., Jan. 24-26, 2005.

[17] B. Wilson, *et al.*, "New and Improved The Broadcast Interfrequency Biases," *GPS World* Sept., 1999, pp. 56-66.

[18] H. Konno, "Analysis of Ionosphere Anomaly Wave Front Impacts on Multiple Satellites," Stanford University, Dept. of Aeronautics and Astronautics, Unpublished Manuscript, October 20, 2006.
<http://waas.stanford.edu/research/PDF/Konno06TechnicalNote.pdf>

[19] Private conversation with Dr. Sam Pullen, October, 2006.

[20] S. Pullen, J. Rife, P. Enge, "Prior Probability Model Development to Support System Safety Verification in the Presence of Anomalies," *Proceedings of IEEE/ION Position Location and Navigation Symposium 2006*, San Diego, CA., April, 2006.

[21] *Global Positioning System Standard Positioning Service Performance Standard*. Washington, D.C., U.S. Department of Defense, October 2001.
<http://www.navcen.uscg.gov/gps/geninfo/2001SPSPerformanceStandardFINAL.pdf>